

Article

Elevation Change Derived from SARAL/ALtiKa Altimetric Mission: Quality Assessment and Performance of the Ka-Band

Quanming Yang, Yuande Yang, Zemin Wang *, Baojun Zhang and Hu Jiang

Chinese Antarctic Center of Surveying and Mapping, Wuhan University, 129 Luoyu Road, Wuhan 430079, China; yangquanming@whu.edu.cn (Q.Y.); yuandeyang@whu.edu.cn (Y.Y.); bjzhang@whu.edu.cn (B.Z.); jianghu@whu.edu.cn (H.J.)

* Correspondence: zmwang@whu.edu.cn; Tel.: +86-027-6877-8609

Received: 17 January 2018; Accepted: 28 March 2018; Published: 1 April 2018



Abstract: The waveform retracking algorithm is a key factor that affects the accuracy of elevation change from satellite altimetry over an ice sheet. The elevation change results from four waveform retracker algorithms (ICE1/ICE2/Sea Ice/OCEAN) provided by the Satellite with ARGOS and ALtiKa (SARAL/ALtiKa) data were compared using repeated SARAL data between March 2013 and April 2016 to determine the optimal retracker in the crossovers of descending and ascending orbits over a Greenland ice sheet (GrIS). The ICE1 provided slightly better results than the three other algorithms with the lowest standard deviation (SD) of 0.30 m year^{-1} . Further comparison was also conducted between the Satellite with ARGOS and ALtiKa (SARAL) and Operation ICEBridge laser data, thereby indicating that ICE1 was the best retracker with an Root Mean Square Error (RMSE) of 0.43 m year^{-1} . The distribution of elevation change rate and uncertainties over Greenland from SARAL were presented using the selected ICE1 retracker with a volume loss of $40 \pm 12 \text{ km}^3 \text{ year}^{-1}$. This volume loss did not include the fast-changing coastal areas of the GrIS. A large thinning was observed in Jakobshavn Isbræ, and a trend that extended far inland was also found from 2013–2016. Furthermore, a melting ice sheet was observed in the large areas northwest over the GrIS.

Keywords: waveform retracking; ICEBridge; SARAL; elevation change; Greenland; slope

1. Introduction

The mass balance of the Greenland ice sheet (GrIS) is an important factor in estimating the rate of increase of global sea levels. The complete melting of the GrIS could increase the global sea level by 7 m, and the state of the GrIS is critical to the survival of humanity [1,2]. Typically, the mass balance of the GrIS is modelled by combining surface mass balance (SMB) from a climate model and ice flux across ice grounding lines from interferometry and other measurements. Such GrIS SMB models may undergo model uncertainties and the inter-annual mass variations of GrIS [3,4]. Currently, the Gravity Recovery and Climate Experiment (GRACE) is the satellite gravimetric mission for GrIS mass balance estimates [5]. GRACE has become a standard tool for monitoring the mass balance of ice sheets since 2002 [6–8]. However, GRACE-based estimations of the mass balance of Greenland typically have spatial resolutions of approximately 300 km and can be further degraded by its systematic errors such as north-south stripes, data noises and errors introduced by the uncertainties of models that represent temporal gravity effects.

Mass balance can also be derived from elevation measurements observed by altimetry missions such as ERS-1, ERS-2, Envisat, ICESat, CryoSat-2 and SARAL. Mass change derived by satellite altimetry characterizes a higher spatial resolution than that observed by GRACE [9,10]. However,

issues such as snow surface penetration and steep terrain in estimating elevation change from satellite altimetry have been acknowledged since the first altimetry mission. The waveform retracking algorithm is an effective approach that tracks the actual surface to reduce the influence of surface penetration and topography [11]. Thus, selecting an appropriate waveform retracker is a key factor in estimating elevation change over the GrIS.

Several approaches based on altimetry data have been used in estimating elevation change. For example, the digital elevation model (DEM) time series [10,12–14], crossover locations [15] and repeat-track (RT) methods [16–18] have been used over ice sheets. Every method of estimating the rate of elevation change can be successfully applied to altimetry data. The DEM time series method demonstrates a high efficiency in computation time to derive the rate of elevation change; however, the accuracy of the elevation change rate is insufficient [13]. The crossover location method exhibits high accuracy; however, the high resolution of this method remains a huge challenge. The RT method is currently considered a favorable method for estimating the rate of elevation change because the rare exactly repeated measurements, which can use all available data to provide an elevation change map with a high resolution, are overcome. Thus, the RT method was used in this study.

The Satellite with ARgos and ALtiKa (SARAL/ALtiKa), which was jointly developed by the French National Space Research Centre and the Indian Space Research Organization, was launched in 2013 as a follow-on mission to the mission of Envisat European Space Agency (ESA). SARAL/ALtiKa is the first mission-carried ALtiKa altimeter with the Ka-band (35.75 GHz). The high frequency of the Ka-band has the strength of a radar signal, but is less affected by snow surface penetration. This capability of the Ka-band is a significant improvement when compared with other radar altimeters for snow surface penetration and enables accurate observations over the GrIS [19]. Thus, the elevation change from SARAL data might have a better performance over the GrIS. However, the accuracy and performance in estimating the elevation change derived from SARAL are unknown.

This study aimed to evaluate the accuracy of the elevation change from four waveform retracker algorithms. The results in the crossovers of descending and ascending orbits over GrIS were compared. Subsequently, a further comparison with ICEBridge results was also conducted. Furthermore, this study aimed to investigate the elevation change of the GrIS derived from SARAL. The results of elevation change from the Ka-band of SARAL/ALtiKa were compared with results from the Ku-band of CryoSat-2 and Envisat.

2. Data and Method

2.1. SARAL Data

SARAL has an orbit inclination of 98.55° and a 35-day repeat period. The mono-frequency Ka-band radar altimeter is the main part of the ALtiKa instrument, which can be used for a negligible or small ionosphere correction at such high frequencies. Simultaneously, snow surface penetration is also reduced. The other advantage of ALtiKa is a reduced antenna beam width and radar footprint. For example, the beam width of the Ka-band is 0.6° , thereby resulting in a rapid attenuation of radar return signal power after reaching the peak. Moreover, the pulse limit of the Ka-band footprint is approximately 1.4 km in radius when compared with 1.7 km of the Ku-band, which can reduce the influence of terrain [20]. Furthermore, the enhanced bandwidth of SARAL with 500 MHz leads to a high vertical resolution [21].

The SARAL data center provides three types of data products, namely the operational geophysical data record (OGDR), the interim geophysical data record (IGDR) and the geophysical data record (GDR). The GDR product, which covered the period from March 2013–April 2016 over the GrIS was used in this study. The GDR product mainly includes the time of measurement, the range from the satellite to surface of the Earth reflection, altitude of the satellite, waveform data and geophysical corrections. Pre-processing of the data was conducted through the quality flags provided in the GDR data. The elevation of the surface of the Earth from four waveform retracker algorithms, namely, ICE1,

ICE2, Sea Ice and OCEAN, was provided by SARAL data [21]. Subsequently, the elevation of the surface of the Earth was rectified by geophysical corrections such as wet troposphere, dry troposphere, ionosphere and sea state bias correction.

2.2. Operation ICEBridge Surface Elevation Change Data

The NASA Operation ICEBridge (OIB) mission has been collecting airborne remote sensing measurements to bridge the gap between ICESat and the upcoming ICESat-2 missions since 2009. Airborne remote sensing measurements operate in Greenland between April and May every year. The airborne payload is the laser altimeter. The airborne tracks are separated by a distance of 40 m and a scan bandwidth of 80 m. The OIB airborne topographic mapper (ATM) L4 data are obtained from repeated flight observations. The observations are located at the crossovers of two flight paths or along a flight line that has been flown before [22,23]. For simplicity, the area of overlap is a square with sides equal to the width of the ATM swath (i.e., 240 m × 240 m square) for the perpendicular crossing, or a regular interval, which is typically 0.5 s of flight, thereby corresponding to 60-m spacing at a nominal 120-m/s flight velocity (i.e., 60 m × 240 m). A mean elevation change estimate within each of the overlapping regions is provided based on the point-to-point differences between the two flights using a maximum distance of 2.5 m. An elevation change estimate can be found only when the number of point-to-point differences (typically more than 500) is sufficient. Martin reported a vertical point-to-point accuracy of 3 cm and a standard deviation (SD) of 2.8 cm year⁻¹ of the L4 elevation change [24]. The elevation changes from the L4 data from 2013–2015 were used to validate the accuracy of elevation change derived from the SARAL data in this study.

2.3. Algorithm for the Elevation Change Estimation from the SARAL Data

The repeat-track (RT) method was used to estimate the rates of elevation change along the SARAL ground track with a resolution of 1000 m. The least-squares regression was performed in the RT method as presented by Flament and Rémy [25] and Légrésy et al. [26]. The seasonal signals were also considered in the model [14,17]. The ground tracks were revisited by the satellite at approximately 35 days and within ±1000 m of the reference track at the Equator. The rate of elevation change for bins spaced at approximately 1000 m along the ground tracks of the satellite was selected for calculation. A bin is a circular area with a given radius, centered at a location along the selected reference track of the satellite. The measurements of elevation from repeated cycles within a given bin were least-square fitted to the space and time function. The elevation change rate was estimated for all the data in 1000-m along-track segments of the satellite track by the RT method. According to the odd and even pass numbers [21], the results of the ascending and descending orbit were extracted from the results of the elevation change rate. The processing scheme is illustrated in Figure 1.

Following [17], the rate of elevation change was estimated. The ranges between the satellite and reflection of the surface of the Earth were corrected based on the different waveform retracking algorithms provided by the SARAL data. Subsequently, the elevations of the reflection of the surface of the Earth were derived as the altitude of the satellite minus the range. Every elevation measurement of the along-track segments of the satellite track in a bin was used to estimate the rate of elevation change. Measurements were conducted five times repeatedly based on the models to estimate the rate of elevation change and investigate the performance of various waveform retrackers.

A least-square regression was used to estimate the parameters [14,17]. The first-round estimated parameters used all of the elevation measurements. The residuals of the measurements and the σ of the residuals were computed. The 3σ outlier rejection was applied subsequently to remove anomalous elevations. If a residual v_i^j was three-times larger than its σ , then the corresponding measurement H_i^j was rejected and the next-round parameter estimation was performed. This step was conducted repeatedly until no further observations were rejected. To constrain each solution, 18 distinct epochs were needed to estimate the parameters. The estimation for a bin where more than 100 data points were available for the fitting procedure after the outlier rejection was provided [27,28]. The minimum

and maximum percentage of outliers were found to be 1.83% for the ICE2 retracker and 3.35% for the OCEAN retracker, respectively. The percentage of outliers was 1.98% for the ICE1 retracker.

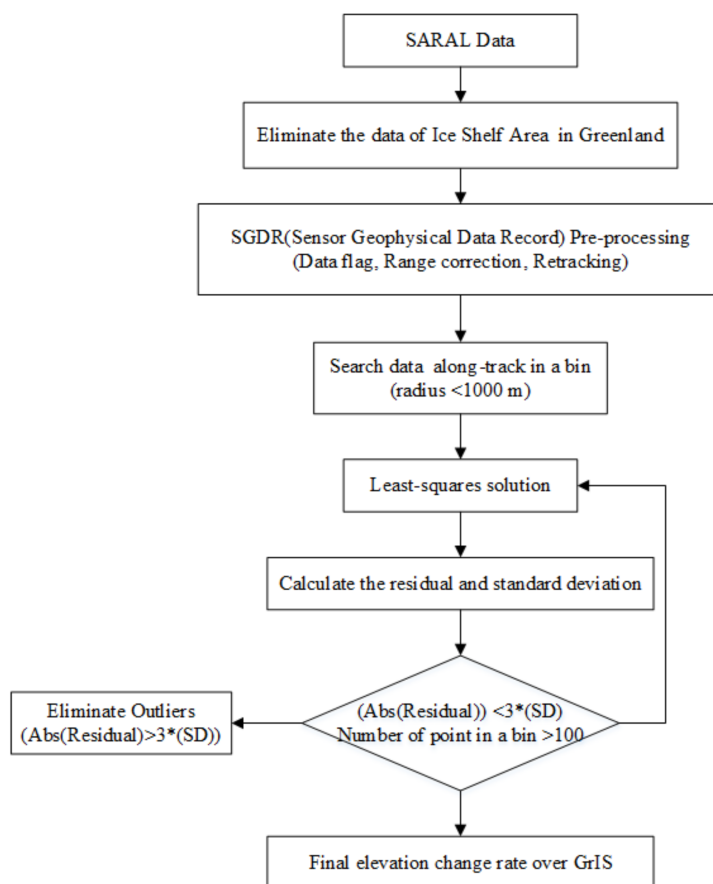


Figure 1. Sketch of the processing scheme to derive elevation change from SARAL over the Greenland ice sheet (GrIS). To constrain each solution, 3σ , 18 distinct epochs and more than 100 points are needed to estimate the parameters in the least-squares regression.

The uncertainties of elevation change were inferred by solving the rate of elevation change that was derived from the least-square fit [29]. The calculation steps of the uncertainties of elevation change rate were as follows. The residuals between the observations and fitted values were estimated based the formulation of Huang et al. [17]. The mean square of weight was inferred from the residuals. The final co-factor matrix of the relevant parameters was also estimated using the law of error propagation.

3. Results

3.1. Crossover Analysis of SARAL

In the same time span from March 2013–April 2016, the elevation change rate of crossovers from ascending and descending orbit should be nearly the same. Thus, the elevation change rate differences at crossovers can reflect the accuracy of SARAL. The rate differences were estimated over the GrIS from 2013–2016. The calculation included five steps: (i) the elevation change rates were estimated by the RT method along-track for all orbits; (ii) the results of elevation change rate for ascending and descending orbits were extracted from results for all orbits; (iii) quadratic polynomials were fitted to derive the approximate location of crossover for the ascending and descending orbits; (iv) the precise location of the crossover was estimated by iteration of (ii) and (iii); and (v) the elevation change rate differences of the crossovers were calculated [30].

The statistics of the elevation change rate differences are displayed in Table 1. The SD of the differences from raw SARAL data was $0.470 \text{ m year}^{-1}$ and ranged from $0.303 \text{ m year}^{-1}$ – $0.365 \text{ m year}^{-1}$ for the four retracers. Of all the retracers, the ICE1 retracker exhibited the optimal performance with the lowest SD of $0.303 \text{ m year}^{-1}$ and the most crossover point numbers of 6595. This result may be due to the applied relocation of the radar return from the ICE1 retracker. Thus, the results from the ICE1 retracker and raw data are discussed as follows.

Table 1. Summary of the differences in the crossovers of descending and ascending orbits from SARAL. For each of waveform retracking algorithm, the bias and SD (standard deviation) of differences in the crossovers are given. The minimum values are highlighted in bold.

	Bias (m year^{-1})	SD (m year^{-1})	Numbers
Raw	−0.018	0.470	6535
ICE1	−0.015	0.303	6595
ICE2	−0.047	0.314	6585
Sea Ice	−0.019	0.348	6548
OCEAN	−0.004	0.365	6515

Figure 2 depicts the elevation change rate differences at the crossovers for the raw and ICE1 retracker data of SARAL. The large residuals in the interior of the GrIS can be observed in Figure 2a. In the interior of the GrIS, the rate differences for the ICE1 waveform retracker were significantly improved, as presented in Figure 2b. However, large differences in the margin regions for the ICE1 retracker were still observed, as demonstrated in Figure 2b. Numerous gaps were observed in the coastal areas of the GrIS in Figure 2.

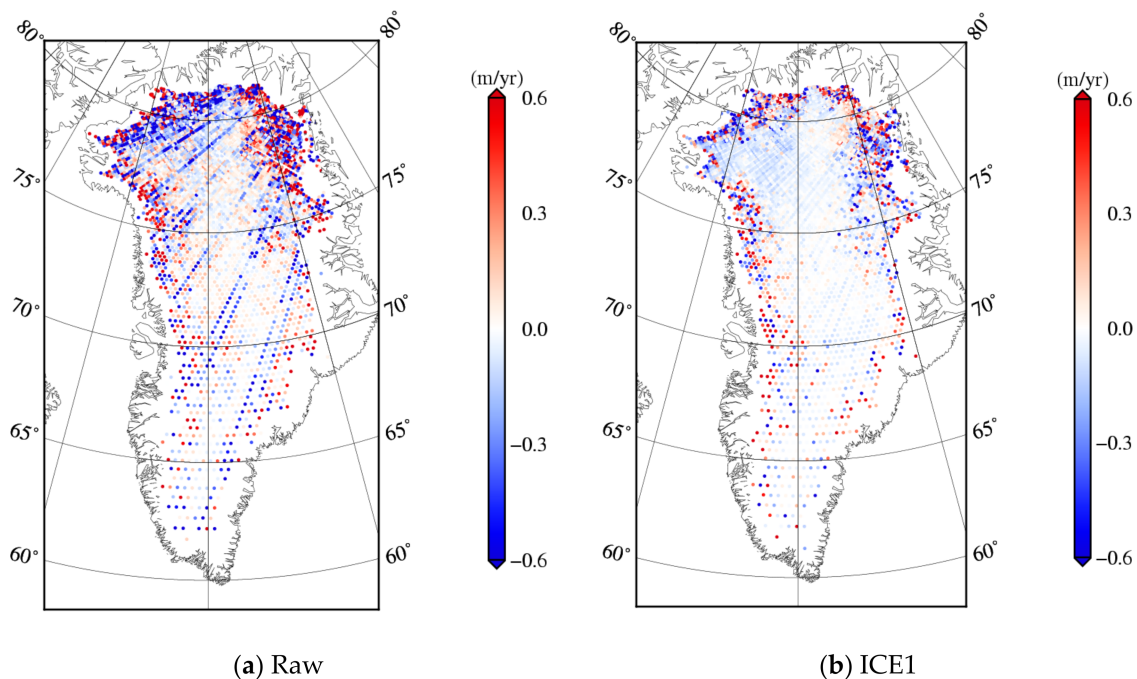


Figure 2. Elevation change differences in the crossovers of descending and ascending orbits from SARAL. (a) The differences of rate in the crossovers from SARAL without waveform retracking (raw). (b) The differences of rate in the crossovers from SARAL with the ICE1 retracker algorithm.

The high surface slope might be an important reason for explaining the rate differences in the margins of GrIS. Figure 3 illustrates the surface slope of the GrIS derived from the ICESat DEM [31]. A significant influence on the return waveform given by the surface slope was recognized [32]. A radar signal will be reflected from the closest point to the satellite and not from a nadir within the footprint of the satellite [33]. Moreover, the return waveform will be complicated in these steep regions and might result in errors in observations. Figure 4 plots the statistics of the comparison in the crossovers as a function of surface slope. The numbers of crossovers decreased with an increase of the surface slope, which was observed in Figure 4 (marked in black asterisks). In Figure 4, the bias in the absolute value of crossovers, which is marked in red for raw and in cyan for the ICE1 retracker, increased with the increase of the slope. This suggests that the slope of the terrain plays an important role in estimating elevation change rates. The gap observed in the coastal areas of the GrIS in Figure 2 might also be interpreted by the influence of topography. The radar mission on SARAL might lose track when the satellite moves from ocean to land, thus leading to few points of the rate in the coastal area of Greenland. Thus, the elevation change rate in the coastal areas of Greenland could not provide an efficient solution based on several current waveform retracker algorithms.

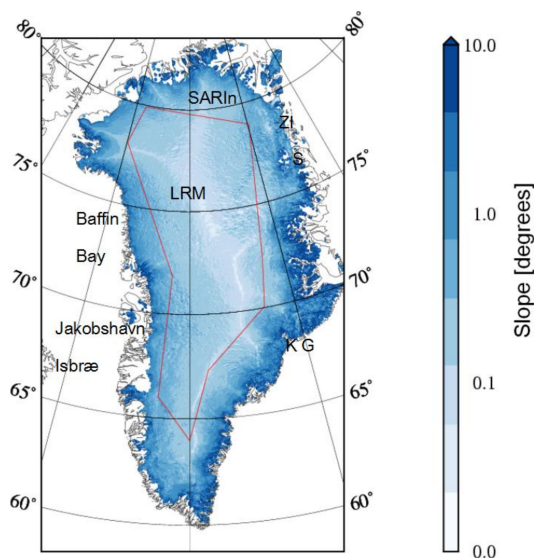


Figure 3. Surface slope of the GrIS derived from the ICESat digital elevation change model (DEM) [31]. The boundary between the Synthetic Aperture Radar Interferometric (SARIn) and Low Resolution Mode (LRM) regions is marked in red based on the division of CryoSat-2 [34]. ZI: Zacharias Isstrømen; KG: Kangerlussuaq Glacier; S: Storstrømmen.

In the interior of Greenland, determining the relocation of the radar return might be an important reason for reducing the rate differences in this area. A remarkable performance with a low surface slope for the ICE1 waveform retracker was found. Figure 3 displays the low surface slope in the interior of Greenland. In Figure 4a,b, the absolute value of bias for the ICE1 retracker (marked in cyan) had smaller values than the results in the raw data of SARAL (marked in red). The bias for slopes that were less than 0.4° was less than 0.3 m year^{-1} for the ICE1 retracker data of SARAL. The bias in absolute value for raw data was much higher in the slopes that were greater than 0.4° than the results in the ICE1 retracker. Moreover, the ICE1 retracker clearly provided less biased estimates of elevation change. Only small differences were observed with the ICE1 waveform retracker in the interior over the GrIS in Figure 2b. Thus, the ICE1 waveform retracker had a favorable performance in significantly reducing the differences in the low surface slope of the GrIS.

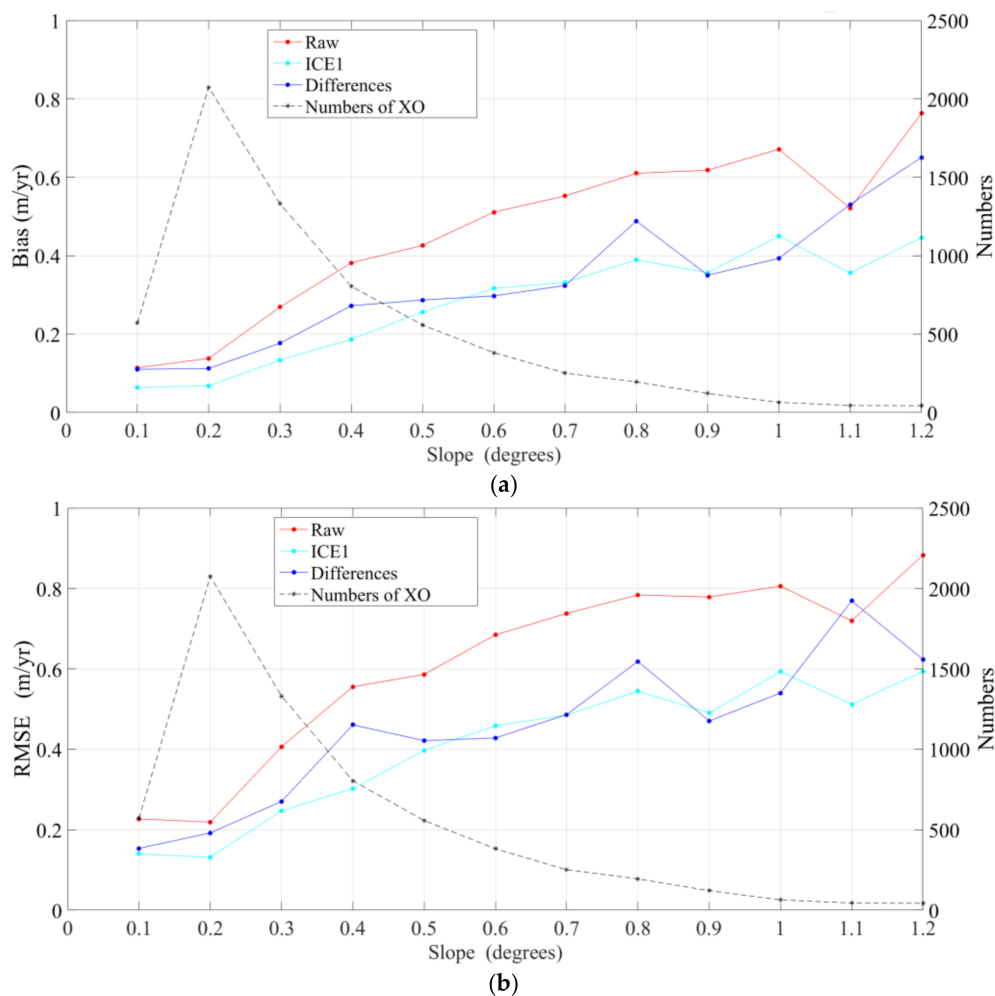


Figure 4. Statistics of the comparison in the crossovers as a function of surface slope marked in red for SARAL data with the ICE1 retracker and in cyan for SARAL data without waveform retracking. Statistics of the differences between SARAL and ICEBridge data as a function of surface slope marked in blue. Bias (a) and RMSE (b) in the slope interval of 0.1° . The black asterisks show the number of crossover points of SARAL data with the ICE1 retracker.

3.2. Accuracy Analysis of Elevation Change Derived from SARAL with Different Waveform Retracker

The elevation change rate derived from the SARAL data for different waveform retracker was also validated against the OIB ATM L4 data. Crossover analysis was unsuitable given the irregular measurements of the ICEBridge in space [32]. The rate of elevation change had a higher spatial resolution from SARAL than from ICEBridge. The OIB ATM L4 data point, as a reference point, was directly compared with points from SARAL. The detailed steps of the approach are as follows. An arbitrary ATM L4 data point was selected as a reference point. Subsequently, the points of elevation change rate derived from SARAL were compared with the OIB ATM L4 data points within a 500-m radius [23]. The final rate differences were estimated between the OIB L4 data and point of SARAL. The elevation change from the SARAL data was divided into two corresponding regions based on the division of CryoSat-2 [34] to further analyze the influence of the topography of different surface slopes. Different surface slopes represented different regions of Low Resolution Mode (LRM) and Synthetic Aperture Radar Interferometric (SARIn). The boundaries of the two regions marked in red are depicted in Figure 3. The statistics of elevation change differences between SARAL and ICEBridge are listed in Table 2.

Table 2. Comparison between SARAL and ICEBridge (airborne topographic mapper (ATM) L4 data). For each waveform retracking algorithm, the bias and RMSE of the differences between the SARAL and ATM L4 data are given. The minimum values are highlighted in bold.

	All			SARIn			LRM		
	Bias (m year ⁻¹)	RMSE (m year ⁻¹)	Number	Bias (m year ⁻¹)	RMSE (m year ⁻¹)	Number	Bias (m year ⁻¹)	RMSE (m year ⁻¹)	Number
Raw	0.18	0.60	13363	0.18	0.67	7291	0.18	0.50	6072
ICE1	0.11	0.43	13604	0.12	0.47	7344	0.10	0.38	6260
ICE2	0.18	0.50	13632	0.22	0.55	7455	0.12	0.41	6177
Sea Ice	0.11	0.46	13516	0.11	0.53	7300	0.11	0.37	6216
OCEAN	0.11	0.49	13417	0.12	0.55	7164	0.10	0.42	6253

All elevation change rate differences are presented as ICEBridge minus SARAL in Table 2. The RMSE of elevation change rate differences ranged from 0.43–0.50 m year⁻¹ between the retracked data from SARAL and the OIB L4 data. The RMSE of the rate differences between raw SARAL and OIB L4 data was approximately 0.60 m year⁻¹. The accuracy of the rate differences for retracked data was better than the results for the raw SARAL data. Over the entire GrIS, of all the retrackers, the ICE1 retracker demonstrated the optimal performance with the lowest RMSE of 0.43 m year⁻¹ and lowest bias of 0.11 m year⁻¹. The RMSE of the rate differences for the ICE1 retracker had been improved from 0.60 m year⁻¹–0.43 m year⁻¹ for the raw data, thereby yielding an improvement percentage (IMP) of 28%. IMP is the ratio between the RMSE of the raw and retracked rate differences and the RMSE of the raw rate differences [17]. The IMP suggests that waveform retracking can reduce the rate differences between the SARAL and OIB L4 data effectively. Moreover, the ICE1 retracker provided slightly better results than the other three waveform retrackers. The rate differences between the SARAL and OIB L4 data were easily amplified by the complicated topography as the return waveform was easily affected by the terrain. This phenomenon suggests that the RMSE of rate differences in different surface slopes might not be the lowest when the same waveform retracker was used.

In the SARIn regions that fell outside the area marked in red (Figure 3), the RMSE of rate differences between the raw SARAL and OIB L4 data was approximately 0.67 m year⁻¹. The RMSE of rate differences after the ICE1 retracker was improved from 0.67 m year⁻¹–0.47 m year⁻¹, thereby yielding an IMP of 30%. The comparison in Table 2 suggests that the ICE1 waveform retracker provided slightly better results than the three other retrackers in the SARIn regions. In the LRM regions that fell within the region marked in red (Figure 3), the RMSE of the rate differences for the raw SARAL data was approximately 0.50 m year⁻¹. The comparison in Table 2 also suggests that the Sea Ice waveform retracker provided slightly better results than the three other retrackers in the LRM regions. The RMSE of rate differences after applying the Sea Ice retracker was improved from 0.50 m year⁻¹–0.37 m year⁻¹, thus yielding an IMP of 26%. Furthermore, the retracked rate differences in the LRM regions improved by approximately 25% over the rate differences in the SARIn regions. This result indicates that the retracked rate differences were more accurate in the LRM areas than in the SARIn areas. The performance after applying the ICE1 retracker was acceptable in these LRM areas with an RMSE of 0.38 m year⁻¹. The aforementioned comparisons (Table 2) denoted that the ICE1 waveform retracker was the optimal retracker among the four retrackers over the entire GrIS. We focused on the elevation change rate after applying the ICE1 retracker to infer several possible causes for the differences between the two missions.

4. Discussion

In this study, the differences between SARAL and ICEBridge were discussed. Figure 5a demonstrates the rate differences between the OIB L4 and SARAL data with the ICE1 retracker. Considerable differences were found in the Northeast Greenland Ice Stream. The influence of topography with high surface slope might be an important cause of the differences. Figure 4 exhibits the statistics of the differences between the SARAL and ICEBridge data as a function of surface slope

(marked in blue). Figure 4a shows the bias of the differences between SARAL and ICEBridge with an interval of 0.1° . The bias in absolute values increased with the surface slope increase. Furthermore, Figure 4b shows that the RMSE of differences also had a higher value with the increase in slope. This result indicates that a high surface slope could result in poor accuracy in the rate differences. Another possible reason for the rate differences might be the influence of distance from the central point of ICEBridge to the measurement point of SARAL. However, no correlation was found between the bias and the point separation. Thus, the influence of the distance threshold could be disregarded.

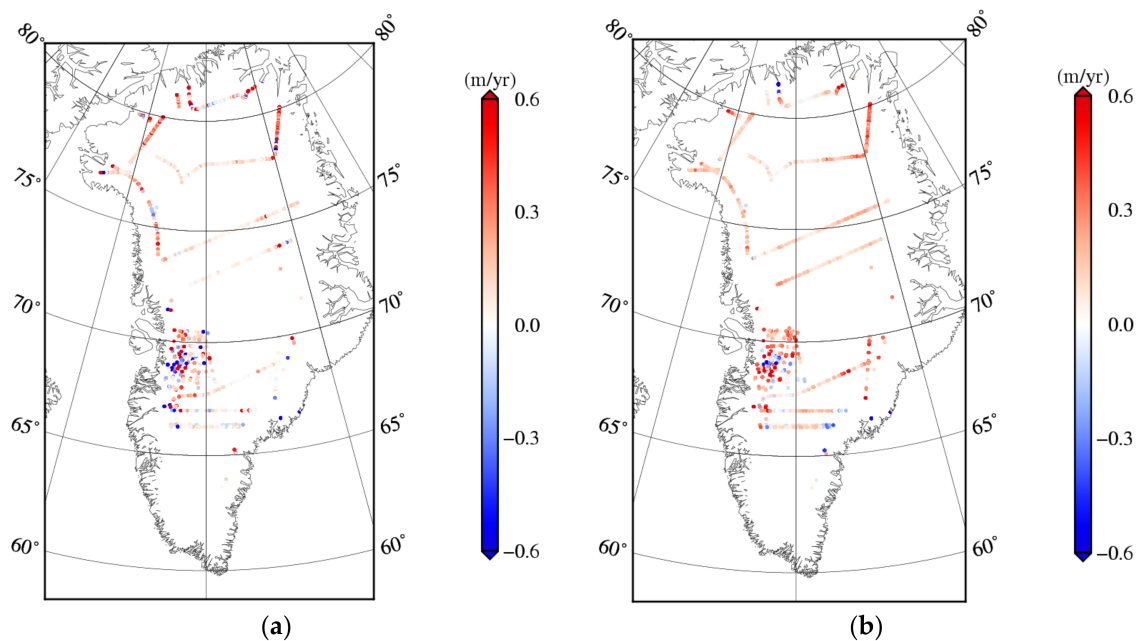


Figure 5. Elevation changes differences between the OIB ATM L4 data and SARAL and CryoSat-2 for 2013–2015. (a) The comparison between OIB ATM L4 data and SARAL. (b) The comparison between ATM L4 data and CryoSat-2.

In this study, we also estimated the mean elevation change rate derived from CryoSat-2 for 2013–2015, according to the method used by Simonsen et al. [23]. In the same period from 2013–2015, the results of rate from CryoSat-2 data were used as a comparison for our results from SARAL. The rate differences between CryoSat-2 and ICEBridge are presented in Figure 5b. Over the whole of Greenland, the rate differences between CryoSat-2 and ICEBridge were estimated with a bias of 0.14 m year^{-1} and RMSE of 0.28 m year^{-1} . Results showed that the rate differences between SARAL and ICEBridge with a bias of 0.11 m year^{-1} were slightly better than the bias of 0.14 m year^{-1} between CryoSat-2 and ICEBridge. The RMSE of rate differences of 0.43 m year^{-1} between SARAL and ICEBridge was slightly worse than the RMSE of 0.28 m year^{-1} between CryoSat-2 and ICEBridge. Similar statistics were also observed in the LRM region of Greenland. The rate differences between SARAL and ICEBridge with a bias of 0.10 m year^{-1} and RMSE of 0.38 m year^{-1} were used as a comparison for the rate differences between CryoSat-2 and ICEBridge with a bias of 0.15 m year^{-1} and RMSE of 0.23 m year^{-1} . The different abilities of snow surface penetration between the Ka-band and Ku-band might be an important reason for the results of different RMSE. The depth of snow surface penetration of the Ka-band is smaller than the Ku-band. The elevation change derived from SARAL was closer to the surface of the ice sheet when compared with the results from CryoSat-2. Meanwhile, SARAL is more subject to weather variability, as Ku-band radars may not see light snowfall events, which are observed by SARAL and ICEBridge. Another possible reason for the results of RMSE is the different orbit densities. The density of CryoSat-2 orbit was much higher than the density of the SARAL orbit. From the result of bias, the Ka-band of SARAL had a better performance than CryoSat-2. This might

suggest that the elevation change rate derived from the Ka-band was a closer reflection of the snow surface change rate than the Ku-band.

The distribution of elevation change derived from the SARAL data acquired from March 2013–April 2016 over the GrIS is exhibited in Figure 6a. The rates of elevation change over the GrIS were estimated from the SARAL data retracked using the ICE1 retracker through the RT method. A clear pattern of thinning (blue) along the margins of Greenland can be observed in Figure 6a. Only a few variations or nearly no change in the interior of the GrIS is depicted in Figure 6a. The pattern generally agreed with the findings inferred from Envisat, ICESat and CryoSat-2 [12,18,23,35,36]. The strong thinning in Jakobshavn Isbræ on the west coast of Greenland was the most prominent and extended far inland. This phenomenon was observed by CryoSat-2 and ICESat [12,14,18,36], thereby presenting the recently large elevation loss in the area of the major outlet glaciers. Kangerlussuaq Glacier (Figures 3 and 6a) is another outlet glacier with large thinning. In the Zacharias Isstrømen (Figure 3), the outlet glacier of the Northeastern GrIS presents a high rate of elevation loss. The trend of thinning in this region extended to approximately 150 km upstream of the Northeast Greenland Ice Stream. The pattern of pronounced thinning was only observed by the CryoSat-2 data [36]. This pattern represented the increase in the speed of Zacharias Isstrømen. Thickening was the most evident near Storstrømmen in the Northeastern GrIS. This phenomenon was consistent with an on-going dynamic response to the identified surge and was previously found based on the ICESat and CryoSat-2 data [12,23,35]. Simonsen previously reported that a slight thickening was also found inland of East Greenland (approximately 75°N) [23]. SARAL showed thinning in the northwestern margins over the GrIS (Figure 6a), thereby confirming the findings over the GrIS that were previously observed by Khan et al. [37] and Sørensen et al. [18].

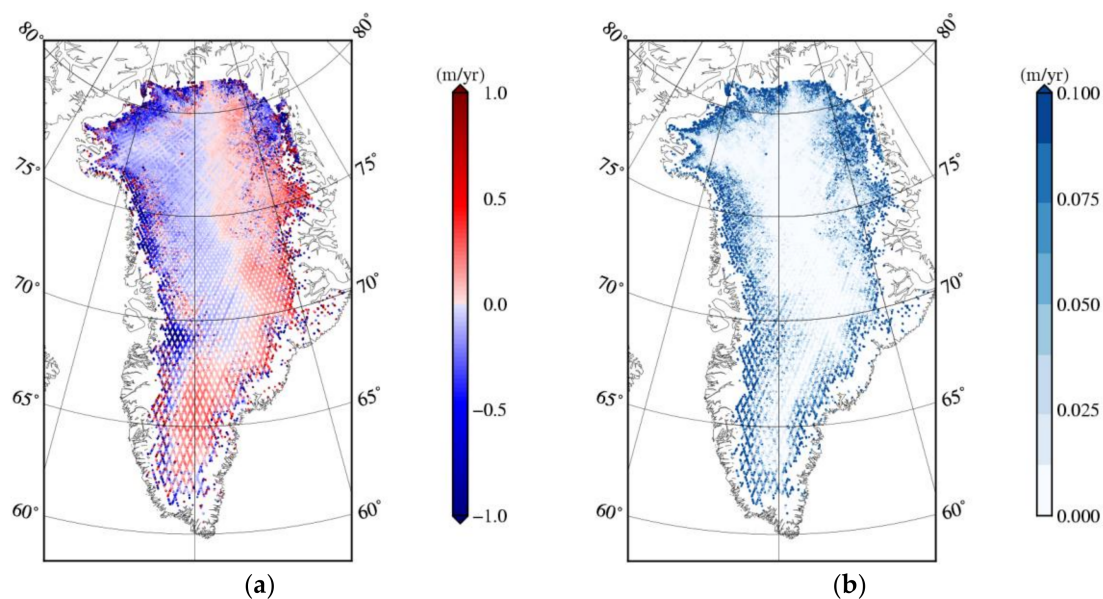


Figure 6. (a) Rate of elevation change over the GrIS derived from 2013–2016 SARAL altimetry with the ICE1 retracker. (b) The corresponding uncertainties of the elevation change rate derived from SARAL with the ICE1 retracker.

The uncertainty of elevation change derived from SARAL was based on the least-square model. This uncertainty can also be inferred in Figure 6b. Low uncertainties in the interior of Greenland can be observed in Figure 3, and most values were less than 1 cm year⁻¹. The high uncertainties were generally observed in the margins over the GrIS. The complicated terrain might be an important reason for the non-perfect relocation and preferential sampling of high points of radar return.

In comparison with previous conventional radar altimeters [12], using SARAL could reduce the footprint to 1.4 km in radius when compared with the Ku-band footprint radius of 1.7 km. The high frequency of the Ka-band (35.75 Hz) also reduced the impact of snow surface penetration. Meanwhile, the waveform retracking algorithm, which tracks the actual surface, was also an effective approach in reducing the effect of surface penetration and topography [11]. The results of elevation change from SARAL data were interpolated onto a 10-km grid for the calculation of volume change [28,38]. The volume change of Greenland derived from SARAL was also estimated with a volume loss of $40 \pm 12 \text{ km}^3 \text{ year}^{-1}$ from March 2013–April 2016. In comparison, a volume estimation of Greenland derived from CryoSat-2 with a larger volume loss of $191 \text{ km}^3 \text{ year}^{-1}$ was found in the time span from 2012–2016 [23]. Due to the use of the new measurement mode of SARAL in SARIn mode, the results of elevation change rate from CryoSat-2 data could provide more values in the fast-changing coastal areas. However, a similar phenomenon of elevation change was found by both SARAL and CryoSat-2. In the northwestern regions of Greenland, large areas of ice sheet thinning were observed by both SARAL and CryoSat-2. Meanwhile, the results from SARAL in this study were compared with the elevation change rate of Greenland derived from Envisat from 2002–2010 [18]. An acceleration of loss of elevation was detected in the northeastern regions of Greenland. In the Northeast Greenland Ice Stream, the speed-up of loss of surface elevation was also found when compared to the results from Envisat. The acceleration of loss of volume in this area was also observed by CryoSat-2 in the time span from 2012–2016 [23]. We also emphasized the underestimation of volume loss derived from SARAL by not measuring the fast-changing coastal areas. Through the comparison with satellites carrying the Ku-band, it suggests that SARAL/ALTiKa helped to investigate the current elevation change of the GrIS.

5. Conclusions

The accuracy of the elevation change results from the four waveform retracker algorithms provided by SARAL data was assessed. The results of rate differences were compared in the crossovers of the descending and ascending orbits over the GrIS from March 2013–April 2016. The ICE1 retracker was a better waveform retracking algorithm given the lowest SD of 0.30 m year^{-1} . The elevation change rate with waveform retracking could significantly improve the accuracy of the elevation change results. The rate differences in the crossovers in the interior of the GrIS were lower than the results in the margins. The slope of the surface topography was considered an important factor for explaining this difference. However, the gap in the margins of GrIS remains unresolved. A possible interpretation is that the radar return onboard SARAL might be disturbed when the satellite moves from the ocean to the steep topography in the coastal areas of Greenland, thereby leading to a few points of the elevation change rate in the coastal area of Greenland.

The elevation change rate derived from SARAL using four waveform retracker algorithms were also validated against the OIB ATM L4 data. The ICE1 retracker determined the lowest rate difference with an RMSE of 0.43 m year^{-1} . However, differences in the elevation change rate between SARAL and OIB ATM L4 data were also found. Several reasons can be used to interpret the rate differences. First, the ICEBridge mission measures only one or two months in Greenland per year. Second, the slope of the surface topography might be another reason. The high slope of surface topography might have large rate differences. The non-perfect relocation and complicated radar returns in the area with high surface slope can be important factors for these differences. Third is the selection of the distance threshold. However, the influence of the distance threshold can be disregarded.

The elevation change rate derived from SARAL was retracked with the ICE1 retracker based on the RT method, which is presented over the GrIS between 2013 and 2016. Simonsen previously reported that a slight thickening was found inland of East Greenland (approximately 75°N) [23]. In Zacharias Isstrømen, the outlet glacier of the Northeastern GrIS presented a rapid rate of elevation loss. SARAL showed thinning in the northwestern margins over the GrIS, thereby confirming the previously-observed findings over the GrIS [18,37]. The volume change of Greenland derived from

SARAL was also estimated with a volume loss of $40 \pm 12 \text{ km}^3 \text{ year}^{-1}$ from March 2013–April 2016. A comparison with the elevation change derived from 2012–2016 [23] CryoSat-2 data was investigated. Large areas of ice sheet thinning were observed by both SARAL and CryoSat-2 in the northwestern regions of Greenland. The acceleration of the loss of surface elevation was also found through the comparison with the results from 2002–2010 [18] Envisat data in this area. Through a comparison with satellites carrying the Ku-band, this suggests that SARAL/ALtiKa can help to investigate the current elevation change of the GrIS. Here, the volume loss from the SARAL data did not include the coastal areas of the GrIS, which are known to account for the majority of the GrIS volume loss.

SARAL/ALtiKa with a high frequency Ka-band (35.75 GHz) and reduced footprint radius of 1.4 km can provide further details of the elevation change over the GrIS, thereby providing a reliable performance. The ICE1 retracker demonstrated its optimal performance when the SARAL data were used to determine the elevation change rate over the GrIS. However, some gaps in the regions from ocean to land were found. An advanced waveform retracker might be required to improve the coverage of elevation change rate in the margins of Greenland.

Acknowledgments: This work was supported by the National Natural Science Foundation of China (Project Nos. 41531069, 41776195).

Author Contributions: Quanming Yang, Yuande Yang, and Zeming Wang conceived of the study, supervised the experiments and improved the manuscript. Baojun Zhang contributed to the analysis and discussion.

Conflicts of Interest: The authors declare no conflict of interest.

References

1. Church, J.A.; Clark, P.U.; Cazenave, A.; Gregory, J.M.; Jevrejeva, S.; Levermann, A.; Merrifield, M.A.; Milne, G.A.; Nerem, R.S.; Nunn, P.D.; et al. Sea-level rise by 2100. *Science* **2013**, *342*, 1445. [[CrossRef](#)] [[PubMed](#)]
2. Dowdeswell, J.A. The Greenland ice sheet and global sea-level rise. *Science* **2006**, *311*, 963–964. [[CrossRef](#)] [[PubMed](#)]
3. Broeke, M.V.D.; Bamber, J.; Ettema, J.; Rignot, E.; Schrama, E.; Berg, W.J.V.D.; Meijgaard, E.V.; Velicogna, I.; Wouters, B. Partitioning recent Greenland mass loss. *Science* **2009**, *326*, 984–986. [[CrossRef](#)] [[PubMed](#)]
4. Rignot, E.; Kanagaratnam, P. Changes in the velocity structure of the Greenland ice sheet. *Science* **2006**, *311*, 986–990. [[CrossRef](#)] [[PubMed](#)]
5. Tapley, B.D.; Bettadpur, S.; Watkins, M.; Reigber, C. The gravity recovery and climate experiment: Mission overview and early results. *Geophys. Res. Lett.* **2004**, *31*. [[CrossRef](#)]
6. Krabill, W.B. *ICEBridge ATM L4 Surface Elevation Rate of Change; IDHDT4_2014-2010_atm_dhdt_greenland*; Technical Report; NASA National Snow and Ice Data Center Distributed Active Archive Center: Boulder, CO, USA, 2014.
7. Sasgen, I.; Dobslaw, H.; Martinec, Z.; Thomas, M. Antarctic snow accumulation variability related to ENSO from GRACE. In Proceedings of the 2010 EGU General Assembly Conference, Vienna, Austria, 2–7 May 2010; p. 1723.
8. Velicogna, I. Increasing rates of ice mass loss from the Greenland and Antarctic ice sheets revealed by GRACE. *Geophys. Res. Lett.* **2009**, *36*, 158–168. [[CrossRef](#)]
9. Jin, S.; Zou, F. Re-estimation of glacier mass loss in Greenland from GRACE with correction of land–ocean leakage effects. *Glob. Planet. Chang.* **2015**, *135*, 170–178. [[CrossRef](#)]
10. Ewert, H.; Groh, A.; Dietrich, R. Volume and mass changes of the Greenland ice sheet inferred from ICESat and GRACE. *J. Geodyn.* **2012**, *59–60*, 111–123. [[CrossRef](#)]
11. Nilsson, J.; Vallelonga, P.; Simonsen, S.B.; Sørensen, L.S.; Forsberg, R.; Dahl-Jensen, D.; Hirabayashi, M.; Goto-Azuma, K.; Hvidberg, C.S.; Kjær, H.A.; et al. Greenland 2012 melt event effects on cryosat-2 radar altimetry. *Geophys. Res. Lett.* **2015**, *42*, 3919–3926. [[CrossRef](#)]
12. Pritchard, H.D.; Arthern, R.J.; Vaughan, D.G.; Edwards, L.A. Extensive dynamic thinning on the margins of the Greenland and Antarctic ice sheets. *Nature* **2009**, *461*, 971–975. [[CrossRef](#)] [[PubMed](#)]
13. Smith, B.E.; Fricker, H.A.; Joughin, I.R.; Tulaczyk, S. An inventory of active subglacial lakes in Antarctica detected by ICESat (2003–2008). *J. Glaciol.* **2009**, *55*, 573–595. [[CrossRef](#)]

14. Sørensen, L.S.; Simonsen, S.B.; Nielsen, K.; Lucaspicher, P.; Spada, G.; Adalgeirsdottir, G.; Forsberg, R.; Hvidberg, C.S. Mass balance of the Greenland ice sheet (2003–2008) from ICESat data—The impact of interpolation, sampling and firn density. *Cryosphere* **2011**, *5*, 173–186. [[CrossRef](#)]
15. Smith, B.E.; Bentley, C.R.; Raymond, C.F. Recent elevation changes on the ice streams and ridges of the Ross Embayment from ICESat crossovers. *Geophys. Res. Lett.* **2005**, *32*, 205–213. [[CrossRef](#)]
16. Frappart, F.; Legrésy, B.; Niño, F.; Blarel, F.; Fuller, N.; Fleury, S.; Birol, F.; Calmant, S. An ERS-2 altimetry reprocessing compatible with ENVISAT for long-term land and ice sheets studies. *Remote Sens. Environ.* **2016**, *184*, 558–581. [[CrossRef](#)]
17. Hwang, C.; Yang, Y.; Kao, R.; Han, J.; Shum, C.K.; Galloway, D.L.; Sneed, M.; Hung, W.C.; Cheng, Y.S.; Fei, L. Time-varying land subsidence detected by radar altimetry: California, Taiwan and North China. *Sci. Rep.* **2016**, *6*, 28160. [[CrossRef](#)] [[PubMed](#)]
18. Sørensen, L.S.; Simonsen, S.B.; Meister, R.; Forsberg, R.; Levinsen, J.F.; Flament, T. Envisat-derived elevation changes of the Greenland ice sheet, and a comparison with ICESat results in the accumulation area. *Remote Sens. Environ.* **2015**, *160*, 56–62. [[CrossRef](#)]
19. Bonnefond, P.; Verron, J.; Aublanc, J.; Babu, K.N.; Bergé-Nguyen, M.; Cancet, M.; Chaudhary, A.; Crétaux, J.F.; Frappart, F.; Haines, B.J.; et al. The benefits of the Ka-band as evidenced from the SARAL/Altika altimetric mission: Quality assessment and unique characteristics of Altika data. *Remote Sens.* **2018**, *10*, 83. [[CrossRef](#)]
20. Armitage, T.W.K.; Ridout, A.L. Arctic sea ice freeboard from Altika and comparison with CryoSat-2 and Operation ICEBridge. *Geophys. Res. Lett.* **2015**, *42*, 6724–6731. [[CrossRef](#)]
21. Bronner, E.; Guillot, A.; Picot, N.; Noubel, J. *Saral/Altika Products Handbook*; No. CNES:SALP-MU-M-OP-15984-CN; CENS: Paris, France, 2013.
22. Studinger. *ICEBridge ATM L4 Surface Elevation Rate of Change*; version 1; Indicate Subset Used; Updated 2017; NASA National Snow and Ice Data Center Distributed Active Archive Center: Boulder, CO, USA, 2014. [[CrossRef](#)]
23. Simonsen, S.B.; Sørensen, L.S. Implications of changing scattering properties on Greenland ice sheet volume change from Cryosat-2 altimetry. *Remote Sens. Environ.* **2017**, *190*, 207–216. [[CrossRef](#)]
24. Martin, C.F.; Krabill, W.B.; Manizade, S.S.; Russell, R.L.; Sonntag, J.G.; Swift, R.N.; Yungel, J.K. *Airborne Topographic Mapper Calibration Procedures and Accuracy Assessment*; NASA: Washington, DC, USA, 2012.
25. Flament, T.; Rémy, F. Dynamic thinning of Antarctic glaciers from along-track repeat radar altimetry. *J. Glaciol.* **2012**, *58*, 830–840. [[CrossRef](#)]
26. Legrésy, B.; Rémy, F.; Blarel, F. Along track repeat altimetry for ice sheets and continental surface studies. In Proceedings of the Symposium on 15 Years of Progress in Radar Altimetry; European Space Agency, Venice, Italy, 13–18 March 2006.
27. Malcolm, M.; Amber, L.; Shepherd, A.; Briggs, K.; Armitage, T.W.; Hogg, A.; Kuipers Munneke, P.; Broeke, M.; Noel, B.; Berg, W.J.; et al. A high-resolution record of Greenland mass balance. *Geophys. Res. Lett.* **2016**, *43*, 7002–7010.
28. Mcmillan, M.; Shepherd, A.; Sundal, A.; Briggs, K.; Muir, A.; Ridout, A.; Hogg, A.; Wingham, D. Increased ice losses from Antarctica detected by CryoSat-2. *Geophys. Res. Lett.* **2014**, *41*, 3899–3905. [[CrossRef](#)]
29. Gunter, B.C.; Didova, O.; Riva, R.E.M.; Ligtenberg, S.R.M.; Lenaerts, J.T.M.; King, M.A.; Van den Broeke, M.R.; Urban, T. Empirical estimation of present-day Antarctic glacial isostatic adjustment and ice mass change. *Cryosphere* **2014**, *8*, 743–760. [[CrossRef](#)]
30. Zhou, X.; Miao, H.; Wang, Y.; Fan, C.; Cui, T. Study on the determination of crossovers by piecewise fitting of satellite ground track. *Acta Geod. Cartogr. Sin.* **2012**, *41*, 811–815.
31. Zwally, H.J.; DiMarzio, J.P.; Brenner, A.C. *Glas/Icesat Antarctic and Greenland Grids*; Digital Media; NASA: Washington, DC, USA, 2012.
32. Brenner, A.C.; Dimarzio, J.P.; Zwally, H.J. Precision and accuracy of satellite radar and laser altimeter data over the continental ice sheets. *IEEE Trans. Geosci. Remote Sens.* **2007**, *45*, 321–331. [[CrossRef](#)]
33. Brenner, A.C.; Blindschadler, R.A.; Thomas, R.H.; Zwally, H.J. Slope-induced errors in radar altimetry over continental ice sheets. *J. Geophys. Res. Oceans* **1983**, *88*, 1617–1623. [[CrossRef](#)]
34. ESTEC. *Cryosat Mission and Data Description*; Technical Report 3; ESTEC: Noordwijk, The Netherlands, 2007.

35. Csatho, B.M.; Schenk, A.F.; van der Veen, C.J.; Babonis, G.; Duncan, K.; Rezvanbehbahani, S.; Van Den Broeke, M.R.; Simonsen, S.B.; Nagarajan, S.; van Angelen, J.H. Laser altimetry reveals complex pattern of Greenland ice sheet dynamics. *Proc. Natl. Acad. Sci. USA* **2014**, *111*, 18478–18483. [[CrossRef](#)] [[PubMed](#)]
36. Helm, V.; Humbert, A.; Miller, H. Elevation and elevation change of Greenland and Antarctica derived from cryosat-2. *Cryosphere* **2014**, *8*, 1539–1559. [[CrossRef](#)]
37. Khan, S.A.; Aschwanden, A.; Wahr, J.; Kjeldsen, K.K. Greenland ice sheet mass balance: A review. *Rep. Prog. Phys. Phys. Soc.* **2015**, *78*, 046801. [[CrossRef](#)] [[PubMed](#)]
38. Zhang, B.; Wang, Z.; Li, F.; An, J.; Yang, Y.; Liu, J. Estimation of present-day glacial isostatic adjustment, ice mass change and elastic vertical crustal deformation over the Antarctic ice sheet. *J. Glaciol.* **2017**, *63*, 703–715. [[CrossRef](#)]



© 2018 by the authors. Licensee MDPI, Basel, Switzerland. This article is an open access article distributed under the terms and conditions of the Creative Commons Attribution (CC BY) license (<http://creativecommons.org/licenses/by/4.0/>).